Design and Hysteresis Modeling of a New Damper Featuring Shape Memory Alloy Actuator and Wedge Mechanism

Duy Q. Bui[1,2], Hung Q. Nguyen[3(✉)], Vuong L. Hoang[2], and Dai D. Mai[4]

[1] Faculty of Civil Engineering, HCMC University of Technology and Education, Ho Chi Minh City, Vietnam
duybq.ncs@hcmute.edu.vn
[2] Faculty of Mechanical Engineering, Industrial University of Ho Chi Minh City, Ho Chi Minh City, Vietnam
{buiquocduy,hoanglongvuong}@iuh.edu.vn
[3] Faculty of Engineering, Vietnamese-German University, Thủ Dầu Một, Binh Duong, Vietnam
hung.nq@vgu.edu.vn
[4] Faculty of Mechanical Engineering, HCMC University of Technology and Education, Ho Chi Minh City, Vietnam
daimd@hcmute.edu.vn

Abstract. This study aims at design and hysteresis modeling of a novel damper featuring shape memory alloy (SMA) to mitigate structural vibrations. The damper consists of SMA springs for actuation and a wedge mechanism to amplify and convert the actuating force into friction against the inner cylindrical face of the damper housing. From the friction between the wedges and housing, the damping force is archived. Following an introduction of SMA spring actuators and SMA dampers, the proposed SMA damper is configured. Experiments are then conducted on SMA springs to obtain their performance characteristics such as transformation temperature, heating time and actuating force. Based on the experimental data, design of the proposed SMA damper is performed and a damper prototype is fabricated. Experimental tests are then conducted to evaluate the damper performance. From the experimental results, hysteresis phenomenon of the SMA damper is presented and investigated. To predict the damper behavior, several hysteresis models are adopted and validated with comparisons and discussions.

Keywords: SMA actuator · SMA spring · SMA damper · Hysteresis model · Structural vibrations

1 Introduction

Material science has attained considerable improvements over the past decades. From the demand for light weight, powerfulness and controllability, smart materials have entered society. Smart materials additionally supply functions such as actuating and sensing to address strict engineering problems by convert reciprocally between mechanical (e.g.,

N. Tien Khiem et al. (Eds.): *Modern Mechanics and Applications*, LNME, pp. 125–136, 2022.
https://doi.org/10.1007/978-981-16-3239-6_10

force, displacement) and non-mechanical (e.g., voltage, temperature) responses [1]. Due to these unique characteristics, smart materials have received numerous interest in the field of structural vibration control.

It is noticeable that conventional suspension systems can help mitigate most engineering oscillations at low resonant frequency. However, they possess unchangeable damping level causing the exciting force to be transmitted greater to contiguous parts and floor at high frequencies, which may lead to noises, uncomfortableness and step–by–step failure of the devices using them. Therefore, semi–active suspension systems that can reasonably adjust damping coefficient corresponding to frequency excitations are desired. A type of smart material that has been widely explored in semi-active suspension systems is magneto-rheological fluid (MRF). MRF contains microscopic magnetic particles suspended within carrier oil. A change in the magnetic field applied to the MRF associates with a change in the fluid viscosity, which leads to damping ability. There are many study works of MRF dampers to solve engineering vibration problems [2–6]. As compared with conventional passive dampers, MRF dampers have remarkable advantages of high damping force, easy control and high reliability. However, the off–state force of the dampers is to some extent high resulting in unwanted formidable oscillations at high frequency excitations. In addition, sealing up the MRF during operating process is a challenging issue as it gives rise to structural complexity of the dampers. High cost of MRF is also a major impediment for the broad application of such dampers in practice.

Another smart material that has been recently investigated to develop damper is shape memory alloy (SMA). SMA has two phases possessing different crystal structures and properties called martensite M (lower temperature) and austenite A (higher temperature). When subjected to particular excitations, SMA experiences a reversible transformation between the two phases to dissipate or absorb energy, which respectively provides applicability for actuating or sensing. In actuating function, SMA can return to its memorized original shape as heated over A_f point (austenite finish temperature), generating a useful force. Inspired by this unique characteristic, several scholars have designed SMA dampers for seismic isolation of engineering structures such as Graesser and Cozzareli [7], Clark et al. [8], Wilde et al. [9], Han et al. [10] and Zuo et al. [11]. The satisfactory research results have shown the promise and potential of such SMA damper kind.

Aiming at simplicity and compactness for installability in small spaces (e.g., suspension systems of washing machine, vehicle), this paper deals with a new damper featuring SMA spring actuator that can produce a high damping force to suppress structural oscillations at low resonant frequency while keeping off-state force small to lessen the force transmission at high frequencies. The characteristics of the SMA springs are first determined through experimental works to serve as an input for calculation, then a damper prototype is designed, fabricated and evaluated. Hysteresis behavior of the proposed damper is analyzed and simulated by some idealized models with comparisons and discussions.

2 Configuration of the SMA Damper

Figure 1 shows configuration of the proposed SMA damper. As shown in the figure, a sleeve shaft slides along a cylindrical housing. Inside the sleeve shaft, a wedge mechanism including an actuating head and four wedges is used to generate friction force against the housing.

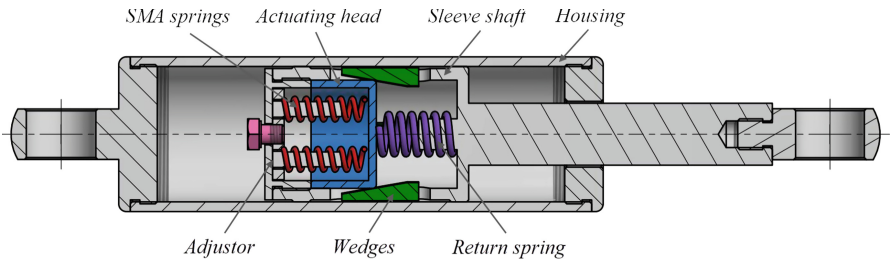

Fig. 1. Schematic configuration of the SMA damper.

When the SMA springs are heated, they extend and push the actuating head to the right. This makes the four wedges move outward in contact with the inner face of the housing. A damping force is produced from the friction between the housing and wedges. Noteworthily, the SMA spring actuator has an inherent disadvantage of low actuating force. In this study, by using a wedge mechanism actuated by an appropriate number of SMA springs, the actuating force from the wedges to the inner face of the housing can be magnified to yield a required damping force. When the SMA springs are cool down, they are contracted to their original shapes and a return spring is employed to push the actuating head back to initial position. The four wedges then move inward and the friction between the wedges and the cylindrical housing is significantly reduced. The damping force and off-state force (the force when the SMA is at ambient temperature of 25 °C) of the SMA damper can be adjusted by using the adjustor.

3 Modeling of the SMA Damper

3.1 Characterization of the SMA Springs

Figure 2 shows the experimental setup to specify characteristics of SMA springs. Two heat insulating pads are used to prevent direct contact between the tested SMA spring and adjacent parts. A DC power supply is employed to provide the spring with a high enough current so that the austenite phase transformation occurs to the finish. Data of force and temperature are transfered from a force sensor and a thermo sensor to a computer through an A/D converter.

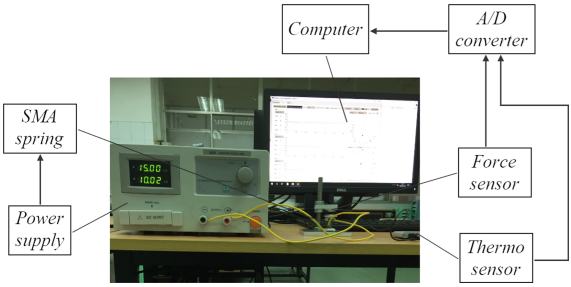

Fig. 2. Experimental setup to specify characteristics of SMA springs.

In this work, three specimens of the SMA springs made by SAES® Getters Group (SmartFlex ® SMA spring) are considered for testing. The geometric dimensions of the springs are given as follows:

– Spring 1: mean diameter 9 mm, wire diameter 0.8 mm, length 15 mm
– Spring 2: mean diameter 6 mm, wire diameter 1.2 mm, length 20 mm
– Spring 3: mean diameter 10 mm, wire diameter 2 mm, length 25 mm

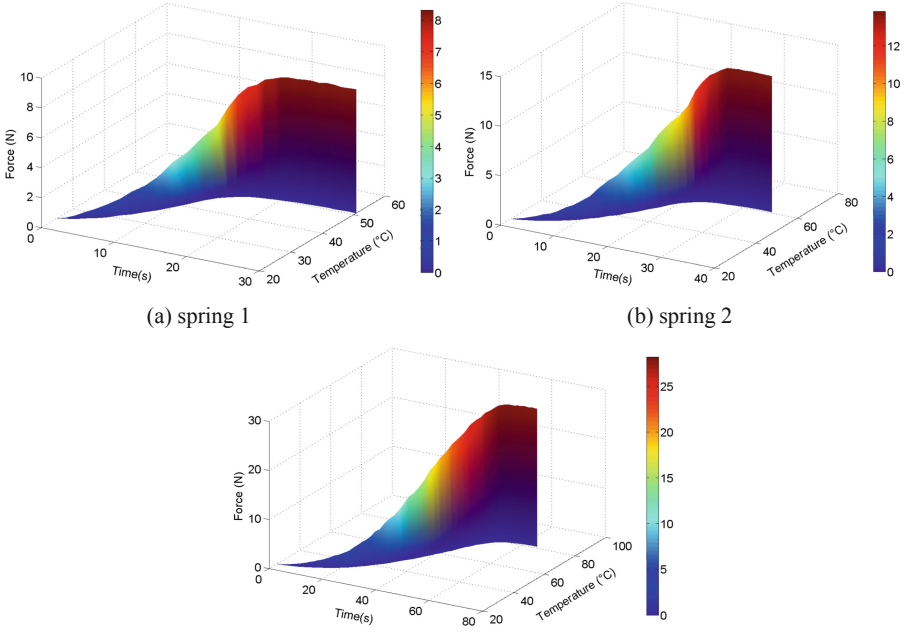

(a) spring 1

(b) spring 2

(c) spring 3

Fig. 3. Experimental responses of the three SMA spring specimens.

The experimental force–temperature–time responses of the three SMA springs are presented in Figs. 3(a–c). As shown in the figures, the actuating force increases with the induced temperature, which is time transient response. At steady state, the maximum actuating forces of the springs 1–3 are respectively about 8.3, 13.8 and 28.1 N. The force saturation of the three springs are almost reached at 20, 26 and 53 s (response time), indicating that the A_f points are approximately 50, 60 and 80 °C, respectively. It is noted that the low response of the SMA spring actuators come from both the time for phase transformation of the SMA material and the time transient response of the excitation temperature. From the results, it can be realized that the spring 1 exhibits the fastest response ability but lowest actuating force while the spring 3 is contrary. In regard to damper size, the spring 2 is the best choice. Considering these data, the design process of the SMA damper is next implemented.

3.2 Design of the SMA Damper

In this section, the SMA damper is designed based on the equilibrium of forces acting on the damper components when the SMA springs are active, as shown in Fig. 4.

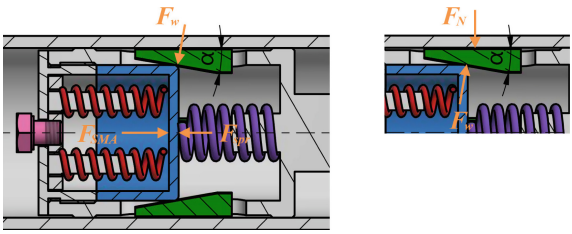

Fig. 4. Equilibrium of forces acting on the actuating head (left) and wedges (right).

As the SMA springs are heated, the actuating force F_{SMA} is generated making the atuating head slide to the right. The sleeve shaft is lubricated on the inner cylindrical face to minimize the friction against the actuating head. By neglecting this friction force, the axial equilibrium equation of the actuating head is given as following

$$F_{SMA} - F_{sp} - F_W \sin\alpha = 0 \tag{1}$$

where F_W is the total force caused by the four wedges and α is the cone angle of each wedge. The restoring force of the return spring F_{sp} is obtained by

$$F_{sp} = k\Delta_{sp} = k\frac{\Delta_w}{\mathrm{tg}\alpha} \tag{2}$$

where k is the return spring stiffness, Δ_{sp} and Δ_w are respectively the displacements of the return spring and wedges. As the four wedges are pushed outward, the reaction force F_N at the contact between the wedges and housing is generated. By neglecting the very small friction between the four wedges and sleeve shaft, the radial equilibrium equation of the four wedges is then obtained by

$$F_N - F_W \cos\alpha = 0 \tag{3}$$

The friction force between the four wedges and housing is determined by

$$F_f = \mu F_N \tag{4}$$

in which μ is the friction coefficient. This friction force is also the on-state damping force F_d of the damper which can be derived by combining the Eqs. (1–3) as follows

$$F_d = \mu\left(F_{SMA} - k\frac{\Delta_w}{\text{tg}\alpha}\right)\text{ctg}\alpha \tag{5}$$

In this study, the material of the housing and four wedges is commercial C45 steel, the cone angle of each wedge α is 10°, the return spring stiffness k is 5 N/mm and the initial thickness of the gap between the wedges and housing is 0.2 mm. With respect to devices owning small assembly spaces, the desired damping force is about 80 to 100 N. From the view of balance between the actuating force, state changing time and damper size, the SMA spring 2 is chosen for our design. To achieve the desired damping force, two SMA springs should be used, which is able to produce a damping force up to 80.8 N.

4 Experimental Test

To verify the proposed SMA damper, a damper prototype is fabricated and its performance is experimentally evaluated. The SMA damper prototype and its components are shown in Fig. 5.

Fig. 5. SMA damper prototype and its decomposed components.

Figure 6 shows the test rig to assess the SMA damper performance. In the system, the linear motion of the shaft is created from the turning motion of a motor through a crank–slider mechanism. The servo motor is controlled by a computer and provides the crank shaft with different constant angular velocities. Once the experiment process is stated, a current of 4 A is applied to the SMA springs. A linear variable differential transformer (LVDT) is employed to record the displacement and a force sensor is used to measure the damping force. From the sensors, the output signals are then sent to the computer via a data acquisition (DAQ).

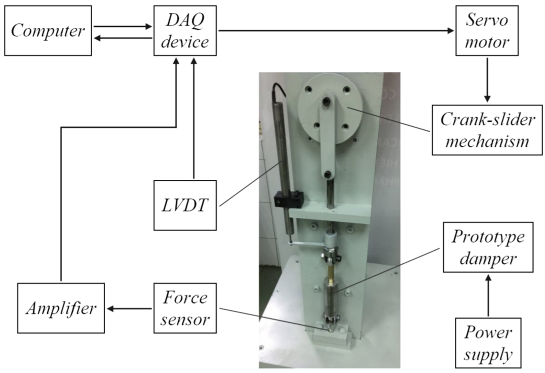

Fig. 6. Test rig to assess the SMA damper performance.

Figure 7(a) represents the responses of the SMA damper prototype in damping force-time relation when the motor rotates constantly at an angular velocity of 4π rad/s (2 Hz). This is also the frequency that the resonance usually occurs. From the figure, it is observed that when the SMA damper is not heated (no current is applied to the SMA springs), the off-state force is about 8 N. This is mainly the friction force between the housing and the shoulders of the sleeve shaft. When the SMA springs are electrically powered, the average damping force is 76.5 N at the steady state, which is about 95% of the theoretical one (80.8 N). Thus, a good correlation is achieved. Moreover, the figure indicates that the rising time to change from the off-state force to the steady value of the damping force is around 25 s, which is consistent to the experimentally measured data of the spring 2 (26 s).

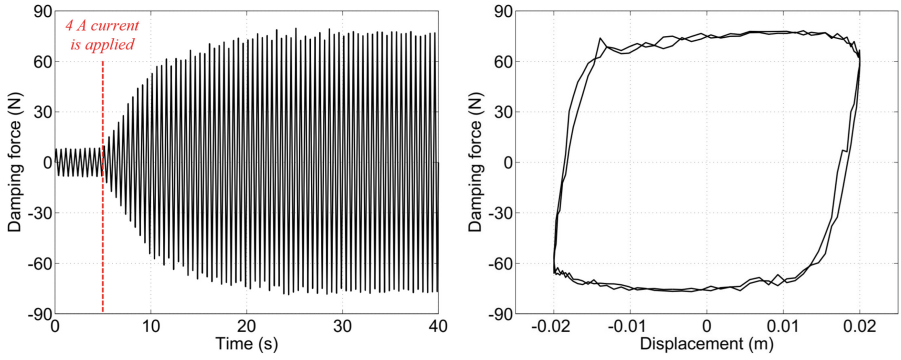

(a) force – time (b) force – displacement

Fig. 7. Experimental step responses of the SMA damper under 2 Hz frequency.

To clearly describe the damping characteristics of the SMA damper at steady state (at which the temperature is around 50 °C), the relation between the damping force and the displacement of the damper shaft over two cycles under the same frequency excitation is obtained, as presented in Fig. 7(b). The hysteresis of the SMA damper, particularly at

the traveling stroke ends, is clearly shown in the figure. It is noted that there is a sudden change of damping force when the shaft motion changes its direction. This is obvious because the damping force of the proposed SMA damper is generated by the friction between the cylindrical housing and the wedges which is almost Coulomb friction.

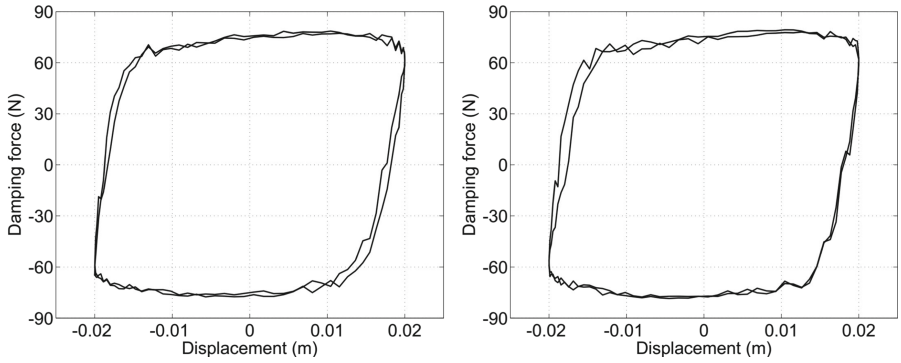

(a) 3 Hz (b) 5 Hz

Fig. 8. Experimental step responses of the SMA damper under higher frequencies.

The same remarks can be derived from Figs. 8(a–b) as testing the damper under higher frequency excitations of 3 and 5 Hz. Minor differences in the off–state force and maximum damping force are admitted as they tend to raise a little with the motor spindle speed, which can be basically explained by the inertial effect of the damper shaft.

5 Hysteresis Model of the SMA Damper

In this research, three hysteresis models including Bingham model [12], Bouc–Wen model [13, 14] and Bui's model [15] are adopted to predict the hysteresis phenomenon of the SMA damper. The three models are in turn mathematically expressed as follows.

Bingham:

$$F_d = c\dot{x} + f_c \mathrm{sgn}(\dot{x}) + f_0 \tag{6}$$

Bouc–Wen:

$$F_d = c\dot{x} + kx + \alpha z \tag{7a}$$

$$\dot{z} = -\gamma|\dot{x}||z|z|^{(n-1)} - \beta\dot{x}|z|^n + A\dot{x} \tag{7b}$$

Bui's model:

$$F_d = c\dot{x} + kx + f_0 + D\sin\left\{C\arctan\left[B(1-E)z + E\arctan(Bz) + H\arctan^7(Bz)\right]\right\} \tag{8a}$$

$$z = \begin{cases} \dot{x} + S_a x \text{ for } \ddot{x} \geq 0 \\ \dot{x} + S_b x \text{ for } \ddot{x} < 0 \end{cases} \tag{8b}$$

where x is the displacement, $\dot{x}$ is the velocity, c and k are respectively the damping and stiffness coefficients, f_0 is the constant bias force, z is an independent variable, and f_c, α, β, γ, n, A, S_a, S_b, B, C, D, E, H are the factors characterizing the hysteresis curve shape. Based on the experimental data, the model parameters are estimated using the curve fitting combined with least square method. The objective function OBJ is to minimize the sum of squared errors between the experimental and predicted damping forces, which is represented by

$$OBJ = \min \sum_{i=1}^{p} \left(F_{m.i} - F_{exp.i}\right)^2 \tag{9}$$

where $F_{m.i}$, $F_{exp.i}$ are respectively the ith predicted and experimental forces, and p denotes the number of calculation points. The estimated parameters of the three models for the 2 Hz frequency excitation are listed in Table 1.

Table 1. Estimated parameters of the three models for the 2 Hz frequency excitation.

Model	Parameter
Bingham model	$c = 142.1$ N.s/m, $f_c = 41.5$ N, $f_0 = 0$ N
Bouc–Wen model	$c = 67.6$ N.s/m, $k = 277.6$ N/m, $\alpha = 1041.5$ N/m, $\beta = 0$ m^{-2}, $\gamma = 278.7$ m^{-2}, $n = 2$, $A = 0.88$
Bui's model	$c = 74.7$ N.s/m, $k = 308.2$ N/m, $S_a = 4.63$ s^{-1}, $S_b = 6.64$ s^{-1}, $B = 13.7$ s/m, $C = 0.93$, $D = 57.1$ N, $E = -0.6$, $H = 2.11$

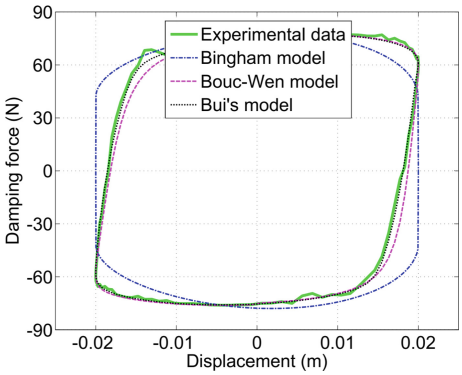

Fig. 9. Comparisons between the predicted and experimentally measured responses under a frequency of 2 Hz.

Using the above optimized parameters, the damper responses predicted by the three models are obtained and compared with the experimental data. Figure 9 show the comparisons between the experimental and predicted damping forces in relation to displacement under 2 Hz frequency. From the figure, it is observed that the three models well adapt the experimentally measured data. Against the others, the Bingham model cannot thoroughly depict the hysteresis behavior of the SMA damper at the two stroke ends; however, it possesses structural simplicity which is beneficial in cases of requiring quick modeling with relative precision such as design for an expected damping force or initial estimation of damper characteristics. On the contrary, the Bouc–Wen model and Bui's model can track the damping force better but are more complicated at the same time; they are thus appropriate to strict cases such as feedback or control designs. More evidences can be found in Figs. 10(a–b) for the higher frequency excitations.

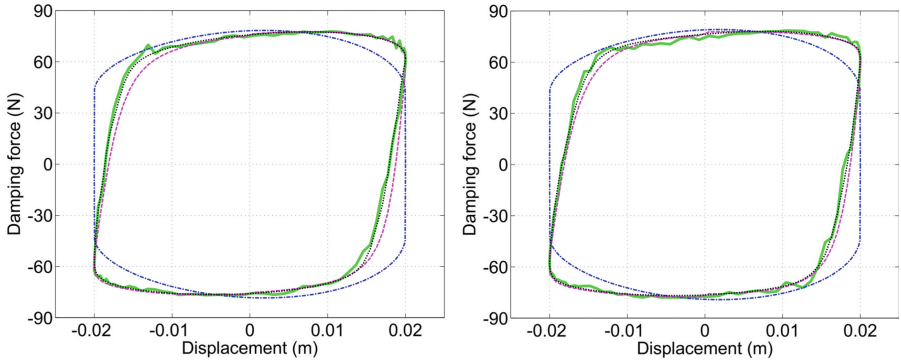

(a) 3 Hz (b) 5 Hz

Fig. 10. Comparisons between the predicted and experimentally measured responses under higher frequencies.

To further assess performance of the three models, errors between the experimentally measured data and each model are quantitatively analyzed. The normalized error of damping force in displacement domain E_x is given by

$$E_x = \sqrt{\frac{\int_0^T \left(F_{\exp} - F_m\right)^2 \left|\frac{dx}{dt}\right| dt}{\int_0^T \left(F_{\exp} - \mu_{\exp}\right)^2 \left|\frac{dx}{dt}\right| dt}} \tag{10}$$

where μ_{exp} are the average experimental forces over the cycle T. The results under different frequency excitations are shown in Table 2. It can be realized that the Bouc–Wen model and Bui's model have higher accuracy in capturing the hysteresis phenomenon of the SMA damper, which mainly comes from the effective and close control of the model physical parameters.

Table 2. Normalized errors between the experimental responses and each model.

Model	2 Hz	3 Hz	5 Hz
Bingham model	0.262	0.268	0.261
Bouc–Wen model	0.074	0.086	0.06
Bui's model	0.03	0.029	0.034

6 Conclusions

This research work contributed to a novel SMA damper for structural vibration control featuring SMA spring actuator and wedge mechanism. After a description of the damper configuration, three SMA springs were tested to specify their characteristics. Modeling of the proposed damper was then conducted based on the experimental data and a damper prototype was designed, manufactured and validated. The results showed that the damper behaves almost like a Coulomb friction damper. The average damping force could reach up to 95% of the calculated value while the off–state force is only about 8 N, which is small enough to prevent most force transmissibility at high frequencies. However, with the state changing time of about 25 s, the damper should be further investigated for effective applicability in closed-loop control systems.

The proposed SMA damper also exhibited the hysteresis behavior in damping force–displacement relation, especially at the stroke ends. To capture this phenomenon, three idealized models consisting of Bingham model, Bouc–Wen model and Bui's model were adopted. Although the Bingham model has lowest accuracy, its simple structure facilitates the modeling which is advantageous to design or premilinary characterization. The Bouc–Wen model and Bui's model control the hysteresis curve more effectively relying on more physical parameters and hence usually prove their abilities in feedback or control designs.

In the next stage of this research, many types of SMA springs and various heating methods will be studied to reduce the actuating time of the damper. In addition, the hysteresis with temperature variable will be investigated for dynamic modeling of the SMA damper.

Acknowledgement. This work was supported by the Vietnam National Foundation for Science and Technology Development (NAFOSTED) under grant no. 107.01–2018.335.

References

1. Lagoudas, D.C. (ed.): Shape Memory Alloys, Modeling and Engineering Applications. Springer, New York (2008). https://doi.org/10.1007/978-0-387-47685-8
2. Carlson, J.D.: Low–cost MR fluid sponge devices. J. Intell. Mater. Syst. Struct. **10**, 589–594 (1999)
3. Nguyen, Q.H., Nguyen, N.D., Choi, S.B.: Optimal design and performance evaluation of a flow–mode MR damper for front–loaded washing machines. Asia Pac. J. Comput. Eng. **1**, 3 (2014)

4. Nguyen, Q.H., Choi, S.B., Woo, J.K.: Optimal design of magnetorheological fluid–based dampers for front–loaded washing machines. Proc. Inst. Mech. Eng. C-J. Mech. Eng. Sci. **228**, 294–306 (2014)
5. Bui, D.Q., Hoang, V.L., Le, H.D., et al.: Design and evaluation of a shear–mode MR damper for suspension system of front–loading washing machines. In: Proceedings of the International Conference on Advances in Computational Mechanics, Phu Quoc Island, Vietnam, pp. 1061–1072 (2017)
6. Bui, Q.D., Nguyen, Q.H., Nguyen, T.T., et al.: Development of a magnetorheological damper with self–powered ability for washing machines. Appl. Sci. **10**, 4099 (2020)
7. Graesser, E.J., Cozzarelli, F.A.: Shape memory alloys as new materials for seismic isolation. J. Eng. Mech. **117**, 2590–2608 (1991)
8. Clark, P.W., Aiken, I.D., Kelly, J.M., et al.: Experimental and analytical studies of shape-memory alloy dampers for structural control. In: Proceedings of SPIE 2445, San Diego, CA, USA, pp. 241–251 (1995)
9. Wilde, K., Gardoni, P., Fujino, Y.: Base isolation system with shape memory alloy device for elevated highway bridges. Eng. Struct. **22**, 222–229 (2000)
10. Han, Y.L., Li, Q.S., Li, A.Q., et al.: Structural vibration control by shape memory alloy damper. Earthq. Eng. Struct. Dyn. **32**, 483–494 (2003)
11. Zuo, X.B., Li, A.Q., Chen, Q.F.: Design and analysis of a superelastic SMA damper. J. Intell. Mater. Syst. Struct. **19**, 631–639 (2007)
12. Stanway, R., Sproston, J.L., Stivens, N.G.: Non-linear modeling of an electrorheological vibration damper. J. Electrost. **20**, 167–184 (1987)
13. Bouc, R.: Modele mathematique d'hysteresis. Acustica **24**, 16–25 (1971)
14. Wen, Y.K.: Method of random vibration of hysteretic systems. J. Eng. Mech. **102**, 249–263 (1976)
15. Bui, Q.D., Nguyen, Q.H., Bai, X.X., et al.: A new hysteresis model for magneto–rheological dampers based on Magic Formula. Proc. Inst. Mech. Eng. C–J. Mech. Eng. Sci. (2020)